A Raman and XPS investigation of supported molybdenum oxide thin films. 1. Calcination and reduction studies

ARTICLE *in* THE JOURNAL OF PHYSICAL CHEMISTRY · OCTOBER 1993

Impact Factor: 2.78 · DOI: 10.1021/j100144a020

A Raman and XPS Investigation of Supported Molybdenum Oxide Thin Films. 1. Calcination and Reduction Studies

Perry A. Spevack* and N. S. McIntyre

Surface Science Western, University of Western Ontario, Laurene O. Patterson Bldg, Western Science Centre, London, Ontario, Canada N6A 5B7

*Received: March 17, 1993; In Final Form: August 9, 1993**

Surface characterization of supported molybdenum oxide thin films is undertaken following calcination and reduction. *In situ* and *ex situ* laser Raman spectroscopy (LRS) and X-ray photoelectron spectroscopy (XPS) are the analytical tools used to probe the catalyst surfaces. Spectral peak broadening of Mo(VI) oxide films has been observed on electrically conducting thin films deposited on active and nonactive surfaces. This peak broadening decreases as the film thickness increases. Reduction of very thin (2 nm) amorphous films of Mo(VI) oxide on planar alumina does not result in lower oxidation states. In somewhat thicker films (4 nm), $Mo_7O_{24}^{6-}$ and a $Mo_6O_{19}^{2-}$ specis are identified following H_2 treatments. Thicker crystalline films (>20 nm) can be reduced into a range of molybdenum oxidation states (XPS) with several phases of oxide present including a nonoctahedral Mo(VI) species and MoO_2. This contrasts with the reduction of bulk MoO_3 where metallic molybdenum is formed under the same reduction conditions.

Introduction

The largest single application of molybdenum-based supported catalysts involves hydrodesulfurization (HDS) processes. Hydrodesulfurization catalysts are used to remove sulfur from petroleum feedstocks before the feedstocks are treated over hydrocracking and other specialized catalysts. The HDS catalyst uses molybdenum oxide frequently promoted with cobalt or nickel oxides and adsorbed on a high surface area support which is usually γ-alumina, although other forms of alumina, carbon, TiO_2, SiO_2, or silica/alumina combinations have been studied.[1-11] The catalyst is calcined and undergoes some form of reduction and sulfidation to activate the material.

Concerning supported molybdenum catalysts only, the first stage of processing usually involves the adsorption of aqueous solutions of molybdenum salts onto a high surface area support.[6,12,13] This is followed by washing, drying, and calcining treatments to obtain a well-dispersed, supported molybdenum oxide precursor of approximately monolayer thickness.[14-16] A variety of supported molybdate species may be found under typical hydroprocessing conditions. The molybdate is usually considered to be in the form of isolated monomers, MoO_4^{2-}, or oligomers, $Mo_7O_{24}^{6-}$, although dimers[17,18] and other polymeric species have sometimes been suggested.[6,10,13,76] Octahedral MoO_3 has been observed at some monolayer and submonolayer catalyst loadings, casting some doubt on the uniformity of coverage.[1,2,18,19] Aluminum molybdate has also been observed as a (undesirable) constituent on alumina-supported catalysts.[18-21] The presence of $Al_2(MoO_4)_3$ resulting from diffusion of molybdate ions into the aluminum oxide lattice suggests that the support/molybdate interaction extends deeper than the proposed monolayer thickness. The nature of the surface molybdate is highly complex and governed by a variety of influences including the structure and composition of the support, the molybdenum oxide precursor and pH of the impregnating solution, the concentration (loading) of the oxide, the calcination temperature, and the storage history of the sample.[6,10,12,13]

This laboratory has been using thin molybdenum oxide films to explore the oxide and sulfide species present during all stages in the preparation of supported molybdenum HDS catalysts.[22-25] In this paper we report surface analytical results of the calcination and reduction processes on such films. In an earlier paper,[22] we described the effects that short duration thermal reduction has on octahedral MoO_3 over the temperature range 350–730 °C. This latter work showed that reduction at temperatures exceeding 600 °C resulted in the formation of crystalline MoO_2 as well as an amorphous oxide containing molybdenum in oxidation states VI, V, and IV. A tetrahedral form of Mo(VI) was also proposed. This present work characterizes thin (≤20-nm) films of molybdenum oxide supported on low surface area (planar) substrates of different chemical reactivities after calcination and reduction treatments. Also, films of octahedral MoO_3 on molybdenum metal (>100 nm) and bulk MoO_3 are reduced under three different gaseous environments at 500 °C for >12 h to determine the products from long-term reduction.

A myriad of techniques have been used in the past to characterize various molybdate structures: gravimetric analysis (GA), electron spin resonance (ESR) spectroscopy, Mössbauer spectroscopy (MAS, MES), UV diffuse reflectance spectroscopy (UVDRS), infrared (IR) spectroscopy, laser Raman spectroscopy (LRS), and X-ray photoelectron spectroscopy (XPS).[2,10,20,22,26-32] Of these, the last two have arguably been the two techniques of choice for the study of supported molybdate catalysts during all stages of processing. X-ray photoelectron spectroscopy (XPS) and laser Raman spectroscopy (LRS) are staple, complementary tools for the catalysis specialist, offering surface sensitivity, chemical speciation, micro- and macroscopic identification, and *in situ* analysis capabilities. For this reason, the present study will use both XPS and LRS for the molybdenum oxide work. Removal of some surface products by chemical dissolution has also assisted in the identification.

Experimental Section

Spectroscopic Analysis. The photoelectron spectrometer used in an in-house modified SSL X-Probe XPS spectrometer, fitted with a custom-designed preparation/reaction chamber and a monochromatized Al Kα X-ray source. The spectrometer is referenced to a Au($4f_{7/2}$) binding energy of 83.93 ± 0.05 eV. Correction of charge shifting of binding energies of the molybdenum films supported on planar alumina was accomplished by referencing their binding energies to 74.5 ± 0.1 eV. On thicker films where photoelectrons from the substrate could not be seen, the binding energies were referenced to the residual hydrocarbon contamination at 284.9 ± 0.1 eV. Any charging detected was sufficiently minor that the use of an electron flood gun was

* Abstract published in *Advance ACS Abstracts*, October 1, 1993.

0022-3654/93/2097-11020$04.00/0

TABLE I: XPS Binding Energies for Molybdenum Compounds

compd	binding energy[a] Mo($3d_{5/2}$)	fwhm	O(1s)[b]	fwhm
Mo(0)	227.8	0.56 (0.77)[c]		
MoO_2	229.2	0.64 (0.74)[c]	529.9	1.1
Mo(IV)	230.1	1.35		
Mo(V)	231.2	1.35		
Mo(VI)[d]	232.7	1.55	530.9	1.3
MoO_3	232.7	1.0	530.6	1.3

[a] BE = ±0.1 eV. [b] Main O(1s) peak. [c] Mo($3d_{3/2}$) component in parentheses. [d] Nonoctahedral environment.

unnecessary. No sample charging was observed on the graphite-supported or molybdenum-supported substrates. Angular-dependent XPS (ARXPS) spectra were taken on selected specimens at normal sample take-off angles of 19° and 90°. The mean sampling depths for these angles are 2 and 6 nm, respectively, based on a λ of 1.95 nm for MoO[33,34] Additional details of the spectrometer may be found elsewhere.[23]

Raman spectra were recorded on a Dilor Omars 89 spectrometer equipped with an optical microscope and an image intensified diode array detector. The macro-sampling mode (~1-mm beam size) was used for the *in situ* analyses, while the microscopic mode (~1-μm beam size) was used for *ex situ* analyses. The spectral sensitivity of the *in situ* analyses was much lower than in the *ex situ* analyses due to the physical geometry of the *in situ* experimental setup. This necessitated the use of much higher laser powers (240–260 mW at the source) and long accumulation times (hours) for the *in situ* analyses compared to the *ex situ* analyses (25–100 mW and accumulation times of several minutes). Samples were carefully monitored for laser beam-induced decomposition. The 476.49-nm line of an argon ion laser was used for vibrational excitation. Spectra were calibrated using a pressed disk of MoO_3 (Alfa products, 99.95%) in KBr as a reference material. The uncertainty in spectral measurements is ±5 cm^{-1}. A base line subtraction routine was used to enhance the Raman peaks in the low-frequency range (<350 cm^{-1}).

XPS Peak-Fitting Procedures. A self-consistent methodology was previously developed for the deconvolution of chemical species from Mo(3d) spectral envelopes following various reduction treatments applied to octahedral MoO_3 films.[22] This procedure has been extended to the present study by including literature data and experimental data from alumina- and graphite-supported oxide compounds prepared during the course of this work and from earlier studies[23,35] (see Table I). Mo(3d) spectra are fitted with an 80% Gaussian/20% Lorentzian peak shape with spin–orbit pair intervals set at 3.15 eV and a spin-orbit area ratio of 1.50 ± 0.01. All spectra were fitted with a sigmoid background developed by Shirley.[36] All binding energies are precise to ±0.1 eV unless otherwise noted.

Quantification of elemental compositions was done by correcting the measured photoelectron peak areas for their calculated cross sections and accounting for the dependence of inelastic electron mean free path on kinetic energy.[37] The molybdenum concentrations were normalized into units of atomic percent. For the Mo(3d) spectral peaks chosen for measurement, these units represent the fraction of molybdenum, relative to the total elemental composition, present in the analyzed region (1000 μm in this case). The atomic percent data can be compared directly with the chemical state information obtained from high-resolution analyses because both sets of information were obtained from the same near surface region sampled by XPS.

Preparation of Oxide Films. Molybdenum oxide films were prepared by two different methods. These methods were chosen to yield two distinct ranges in film thickness: (1) thin (<1–20 nm) molybdenum oxide films deposited on low surface area supports of planar alumina or graphite. Planar alumina and graphite have very different chemical reactivities on which to study metal/support interactions. The second method involved the use of thick (>100-nm) octahedral MoO_3 films supported on molybdenum metal. In the first method, a sputter deposition system with a saddle-field ion source and a planetary stage was used with a high-purity molybdenum target (99.97%) to prepare thin metal films of uniform thickness. An oxide film was grown by heating the metal in air at 200–260 °C for periods of 4 h or longer. Film thicknesses were measured by sputter depth profiling on a scanning Auger multiprobe. In the second method, ~1-cm^2 coupons of high-purity molybdenum metal (99.97%) were cleaned in methanol and then ion sputtered with Ar^+ to activate the surface. The samples were heated as above to yield thick films of octahedral MoO_3 as confirmed by XPS and LRS measurements. An additional oxide sample was prepared as a pressed disk of MoO_3 (Alfa products) using a KBr press using a force of (0.9–1.0) × 10^5 kPa.

Sample Reduction. Thermal reduction was accomplished using H_2 or N_2 gases or by *in vacuo* heating. A different experimental apparatus was used with each thermal treatment. H_2 reduction was carried out in a previously described[22] quartz tube reactor with an optical flat on one end to allow *in situ* Raman spectroscopic measurements. For N_2 reduction, an *ex situ* arrangement was selected wherein the sample rested within a heated quartz tube through which the gas (dry N_2) flowed. The *in vacuo* reduction was carried out in an ultrahigh-vacuum (UHV) preparation chamber of the X-Probe spectrometer (base pressure 1 × 10^{-7} Pa), followed by direct sample transfer under vacuum to the spectrometer chamber. Temperatures for all reduction experiments are accurate to ±5 °C, and all reduction times were at least 12 h in length unless otherwise noted. All transfers of samples following *in situ* reduction were carried out under an inert atmosphere of dry N_2 or Ar via a glovebag[38] to the XPS introduction chamber for further analysis.

Aqueous Ammonia Treatments. Aqueous ammonia has been shown to be effective in selectively dissolving octahedral MoO_3 in the presence of other molybdenum oxide species.[17,18,30,39] A 3 vol % aqueous ammonia solution was prepared by diluting stock ammonia solution with distilled and deionized water to the appropriate concentration. The freshly made solution was then deaerated with a dry nitrogen bubbler for 1 h prior to (and during) the 1-h dissolution experiment. Following dissolution, samples were transferred under inert atmosphere (see above) for XPS analysis.

Results

Analysis of Calcined Thin Films. Following calcination, the structures of the thin oxide films supported on alumina and graphite were studied. Thin molybdenum oxide specimens (≤20 nm) supported on planar alumina were analyzed using the micro-Raman mode. Most of the areas examined by LRS indicate the presence of amorphous surface molybdate structures with a broad spectral peak centered at ~950 cm^{-1} [20,28,29,39,40] (Figure 1). These same features are observed over a range of molybdenum oxide thin films up to ~15 nm in thickness. The peak breadth and position are consistent with previous Raman data[20,28] of low loadings of amorphous, hydrated molybdates supported on alumina substrates at low loadings. The broad peak centered at ~950 cm^{-1} is due to the ν(Mo–O) stretching frequency found for octahedral surface molybdates.[28] Close examination of the sample disks revealed a few crystalline features associated with scratches on the carrier (alumina) surface. Raman spectra of these areas exhibited sharp peaks at 996, 821, and 668 cm^{-1}; these spectral features correspond to octahedral MoO_3.[21,22,40–42] Samples with thicknesses ≥20 nm exhibited Raman spectra corresponding solely to octahedral MoO_3.

The corresponding X-ray photoelectron (XP) spectra (Figure 1a) indicate a single spin–orbit pair centered at BE = 232.7 eV, whose peak width increases as the thickness of the molybdenum

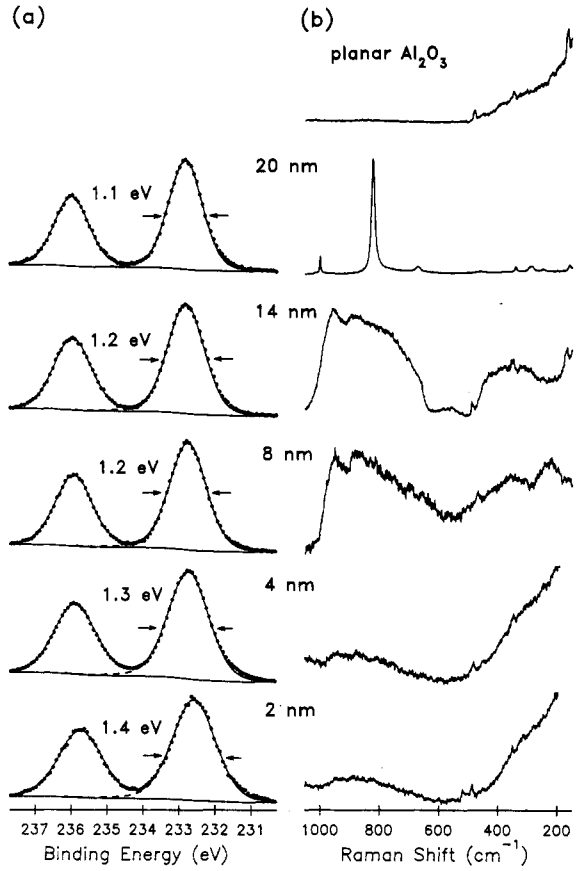

Figure 1. (a) Mo(3d) spectra of molybdenum oxide/planar alumina thin-film catalysts following calcination at 200 °C for 4 h. Peak widths (fwhm) are marked with arrows. Only Mo($3d_{5/2}$) peaks are shown for clarity. (b) Corresponding *ex situ* Raman spectra of (a). Spectra are not corrected for instrument response. Planar alumina substrate is shown for comparison.

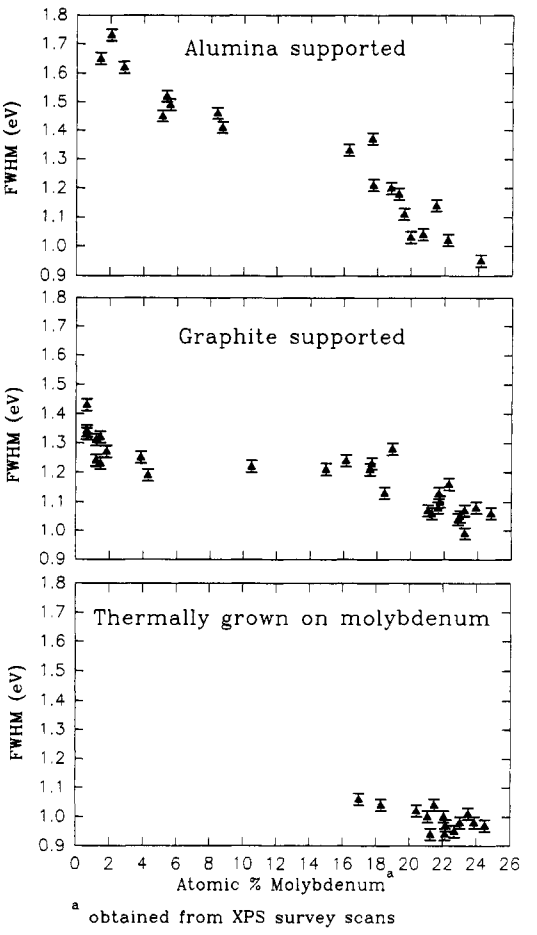

Figure 2. Comparison of Mo(VI) peak widths (fwhm) vs surface molybdenum concentration (expressed as atomic percent molybdenum) for planar alumina-supported, graphite-supported, and thermally grown (Mo(VI)/Mo) molybdenum oxides.

oxide layer decreases. A series of supported molybdenum oxide films were deposited on planar alumina (nonconducting) substrates and graphite (conducting) substrates. Thick (>100-nm) oxide films were also grown on molybdenum metal substrates. The effect of film thickness on the Mo(3d) peak widths (fwhm) is shown in Figure 2. Mo(3d) peak widths in deposited films on planar alumina and graphite show a decrease in fwhm with increasing thickness, but the effect is more pronounced on alumina. However, in the case of alumina substrates, some of the peak broadness may be due to charge-induced broadening of nonconducting samples associated with the photoemission process. In the case of graphite, however, charge-induced broadening is definitely not present. For oxide thicknesses ≥10 nm, the fwhm remains constant at 1.1 ± 0.1 eV. This is comparable to thermally grown films on molybdenum (>100 nm) which all show a constant fwhm of 1.00 ± 0.05 eV. Thus, it appears that the amorphous Mo(VI) oxide film has a Mo(3d) XPS spectrum whose line width is greater than that for octahedral MoO_3 even though their peak centroid positions are identical.

Previous work[17] has indicated that both the calcination time and temperature can have an effect on the molybdenum oxide structure on γ-alumina supported catalysts. In order to explore this idea for planar alumina-supported substrates, two alumina-supported samples were calcined at two different temperatures for two different times: one, an amorphous thin molybdenum oxide film (2 nm) and the other, a thicker crystalline film (20 nm). Figure 3a,b shows Raman spectra of the amorphous and crystalline samples, following air calcination at 200 °C for 4 h, while Figure 3c,d shows spectra of the same two samples following 18 h of air calcination at 300 °C. At 200 °C, the spectrum showed the thinner film to be amorphous molybdate, while the spectrum of the thicker film closely resembled that of crystalline

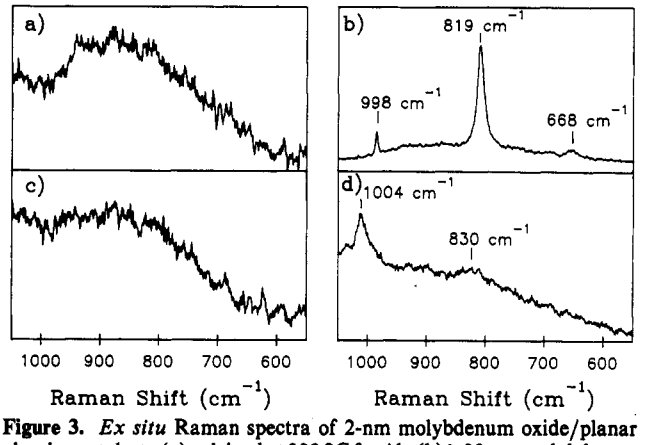

Figure 3. *Ex situ* Raman spectra of 2-nm molybdenum oxide/planar alumina catalyst: (a) calcined at 200 °C for 4 h, (b) ≥20-nm molybdenum oxide/planar alumina catalyst calcined at 200 °C for 4 h, (c) sample (a) further calcined at 300 °C for 18 h, and (d) sample (b) further calcined at 300 °C for 18 h. Note: spectra have not been corrected for instrumental response.

MoO_3. The thinner film remains amorphous after the extended calcination period while the thicker film has transformed from octahedral MoO_3 into a mixture of $Al_2(MoO_4)_3$ (peaks at 1028 (sh), 1004 (s), 830 (w), and ~370 cm^{-1} (w,br))[2,17,20,40] and amorphous molybdate (broad envelope extending from ~950 to 600 cm^{-1}). The 2-nm amorphous oxide film thus appears unchanged by calcination conditions that convert thicker films into $Al_2(MoO_4)_3$.

Dilute aqueous ammonia has been previously shown to selectively dissolve octahedral MoO_3 alone or in the presence of

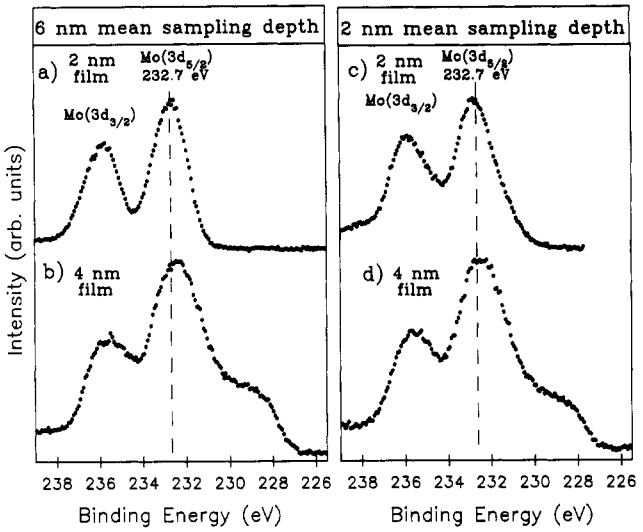

Figure 4. Angle-dependent (ARXPS) Mo(3d) spectra of planar alumina thin-film molybdenum oxides following H_2 reduction at 350 °C for ≥9 h. Spectra are taken at sampling depths of ~6 nm (a, b) and 2 nm (c, d). (a) and (c) 2 nm thick molybdenum oxide; (b) and (d) 4 nm thick molybdenum oxide.

additional oxides, including tetrahedral species.[17,18,30,39] To verify that this treatment is effective, a ~10-nm octahedral MoO_3 film supported on graphite was treated with aqueous ammonia. XPS analysis after treatment (not shown) found that all molybdenum was removed except for a trace amount, which was comprised of a single broadened spin–orbit doublet. On the basis of the results above, this residual molybdenum is necessarily not octahedrally coordinated and may be a tetrahedrally coordinated species.

Reduction of Thin-Film Molybdenum Oxides. X-ray photoelectron spectroscopy was used to examine the effects of thermal reduction in flowing hydrogen of thin film molybdenum(VI) oxides supported on planar alumina. Samples of ~2 and 4 nm thick oxides were reduced in H_2 for over 9 h at 350 °C and transferred under dry nitrogen into the spectrometer for analysis. The Mo(VI) precursor oxides for the 2- and 4-nm specimens are shown in Figure 1. Photoelectron spectra were taken at deep and shallow sampling depths using angle-dependent XPS (ARXPS). The Mo(3d) spectra in Figure 4 shows that, for the 2-nm sample, there is no evidence of reduction of the Mo(VI) oxidation state to lower oxidation states, even at the outermost surface. The slight broadening of the Mo(3d) spectrum at the shallow take-off angle is due to sample charging associated with the alumina and not due to the presence of an additional species. The charging effect is less pronounced at the deeper take-off angle where secondary electrons generated in the underlying aluminum by the X-ray flux can neutralize the insulating overlayer. Similar spectral broadening was observed in the Al(2p) and C(1s) spectra recorded at the shallow take-off angle. The thin film results contrast with the behavior of thicker octahedral MoO_3 films,[22] which exhibited reduced oxidation states after only 1 h of thermal reduction. Curve-fitting the Mo(3d) spectrum of the 4 nm thick film following reduction shows the presence of lower oxidation states (Mo(IV) and Mo(V)) and a contribution from Mo(VI) oxide. The angular-dependent spectra taken for each thin film specimen indicate that the samples are uniformly reacted over the range of depths studied.

In situ Raman spectra (not shown) for the 2 nm thick film (see XPS above) following hydrogen reduction at 350 °C did not reveal any features present on the sample. It is unknown whether the experimental setup was too insensitive to detect any species on such a thin film or whether any detectable species were actually present. Exposure of the 4-nm molybdenum oxide/planar alumina film to a reducing environment at 350 °C yielded largely crystalline compounds as analyzed by *ex situ* LRS (Figure 5). The majority of the areas analyzed on the sample resemble the spectrum in

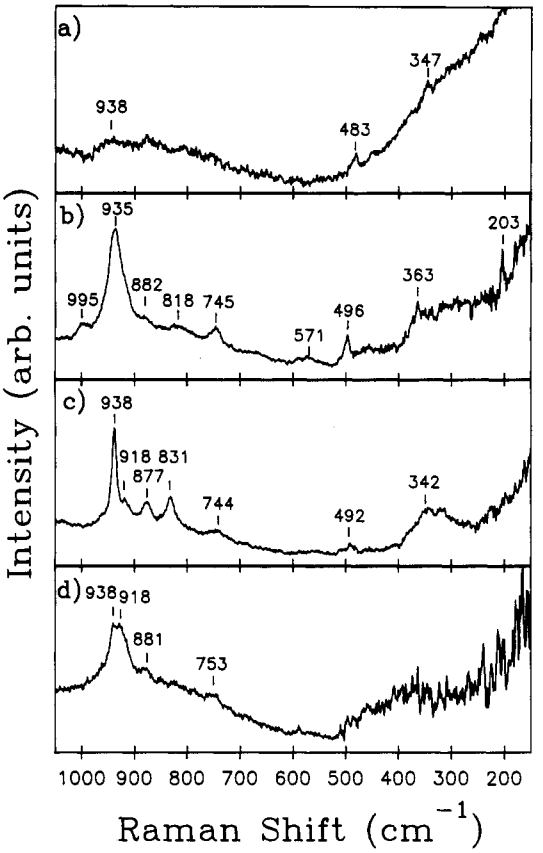

Figure 5. The ~4-nm molybdenum oxide/planar alumina thin-film catalyst reduced in H_2 for 9 h at 350 °C: (a) prior to reduction; (b)–(d) series of *ex situ* LR spectra taken of crystalline areas observed under the optical microscope.

Figure 5b. However, as spectra c and d indicate, the main peak at 935 cm^{-1} in Figure 5b appears to be a convolution of two narrower overlapping peaks at 938 and 918 cm^{-1}. Since this is the spectral region where the symmetric Mo–O stretching frequency occurs for molybdates,[2] the presence of these two species indicates that at least two molybdate species are present. The molybdate $Mo_7O_{24}^{6-}$ is identified on the basis of sharp peaks at 938 cm^{-1} and spectrum c.[2,17,31,40] An oligomer of slightly shorter chain length, such as $Mo_6O_{19}^{2-}$,[43] is also present (peak at 918 cm^{-1} and spectrum d). The frequency of this ν(Mo–O) band is believed to increase with increasing oligomer chain length.[2] There is also evidence of reduced molybdenum species present in some of the spectra in the form of MoO_2[22,31,40,44] with peaks at 745, 571, 496, 363, and 203 cm^{-1}.

Extended Reduction of Octahedral MoO_3. Previous literature has reported[17] that extended reduction (~12 h) at 500 °C will reduce octahedral MoO_3 completely to MoO_2. Our earlier XPS and LRS studies of octahedral MoO_3, reduced for 1 h at 350–730 °C, yielded a mixture of oxides.[22] Extended reduction of octahedral MoO_3 was carried out in this work in an attempt to follow the further evolution of reduction products. Figure 6 results show XPS and Raman data following 14 h of H_2 reduction at 500 °C on a sample of octahedral MoO_3 grown on Mo metal. The XPS spectrum (Figure 6a) shows a mixture of oxidation states present from Mo(VI) to Mo(IV) with MoO_2 (binding energy (BE) = 229.2 eV) accounting for only ~30% and some Mo(VI) oxide (BE = 232.7 eV) still present. However, the *in situ* Raman spectrum of the sample (Figure 6b) indicates no MoO_3; therefore, the Mo(VI) is associated with another hexavalent structure. The reduction experiment was repeated on a fresh sample decomposed in flowing N_2 at 500 °C for $13^1/_4$ h. A mixture of oxides was again seen with Mo(VI) oxide still present. A third sample was prepared and heated *in vacuo* for 13 h at 500 °C and examined but yielded a similar composition to the other two treatments.

TABLE II: Comparison of Surface Composition vs Reduction Treatment for Three Molybdenum-Supported Octahedral MoO_3 Samples; Values Obtained from Mo(3d) Narrow Scan Analyses

	composition (%)[a]			
reduction treatment	MoO_2	Mo(IV)	Mo(V)	Mo(VI)
hydrogen	29	18	26	26
nitrogen	32	21	28	20
in vacuo	35	21	30	14

[a] $\Delta = \pm 10\%$.

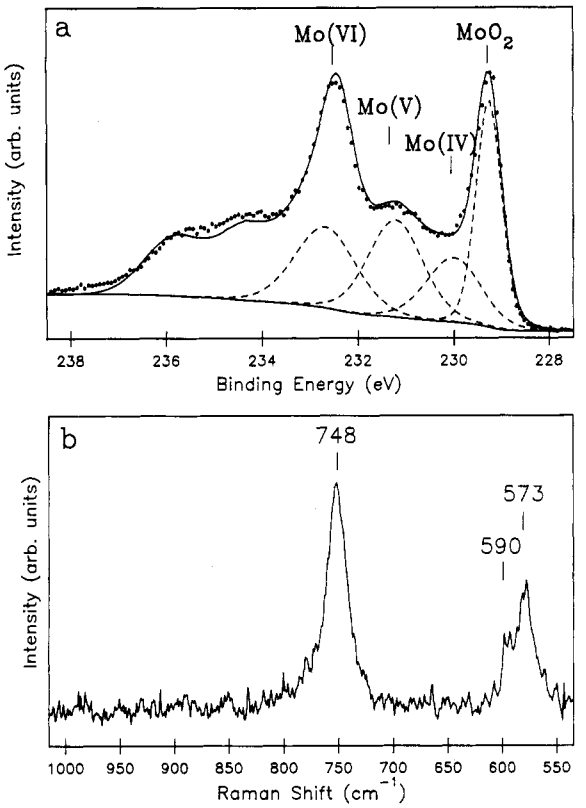

Figure 6. (a) Mo(3d) XPS spectrum of octahedral MoO_3/Mo reduced in H_2 at 500 °C for 14 h. Only $Mo(3d_{5/2})$ components are shown for clarity. (b) Corresponding *in situ* Raman spectrum taken prior to XP analysis.

Quantitative curve fittings of the XPS Mo(3d) envelopes from the three reduction experiments are tabulated in Table II.

To determine whether the reduction procedure was sufficiently long to reduce all of the octahedral MoO_3, a sample of octahedral MoO_3 which underwent 14-h H_2 reduction at 500 °C (see Figure 6b) was treated with aqueous ammonia for 1 h. This treatment (see Figure 7) resulted in a decrease in the concentration of the Mo(VI) component from ~25 to ~15% Mo(VI). The remaining Mo(VI) in the spectrum is therefore *not* MoO_3. The remaining presence of the lower oxide species, Mo(V) and Mo(IV), indicates that even the 14-h reduction period was insufficient to reduce all of the octahedral MoO_3 into a single oxidation state. Similar results (not shown) were found for octahedral MoO_3 after decomposition in nitrogen for >13 h at 500 °C.

To study the effects of support interactions which may be present in the above experiments, an unsupported sample was prepared using a pressed pellet of MoO_3 powder. This sample underwent ~$15^1/_2$ h of H_2 reduction at 500 °C. Following this treatment, the sample was fractured lengthwise under inert atmosphere to permit XPS examination of the outer and inner surface. The results presented in Figure 8 show that the outer surface (Figure 8a) is dominated by a $Mo(3d_{5/2})$ peak at BE = 227.8 eV, fwhm = 0.56 eV which corresponds to metallic

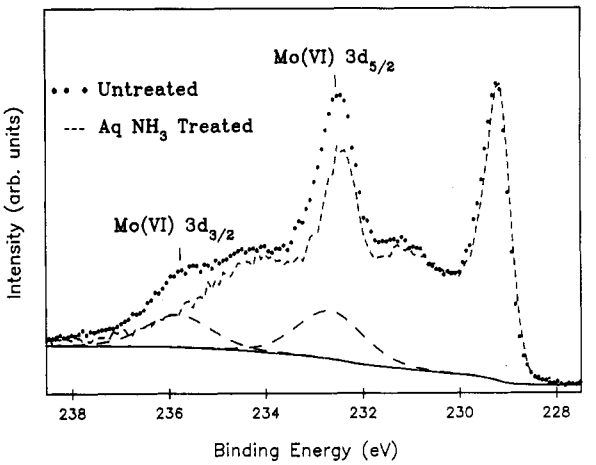

Figure 7. XPS Mo(3d) overlay of molybdenum-supported octahedral MoO_3 reduced in H_2 for 14 h at 500 °C before (dots) and after (dashed lines) aqueous ammonia treatments. Mo(VI) spin–orbit components are curve-fitted and marked in the figure.

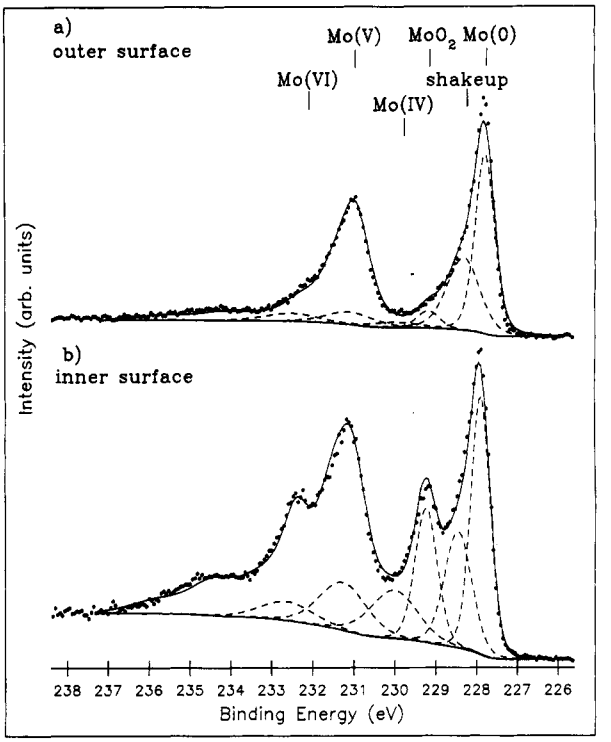

Figure 8. Mo(3d) spectra of a pressed pellet of octahedral MoO_3 following ~$15^1/_2$ h of H_2 reduction: (a) outer surface, (b) inner surface. Only $Mo(3d_{5/2})$ spin–orbit components are shown for clarity.

molybdenum.[45-47] The inner surface (Figure 8b) shows evidence of some MoO_2 as well as Mo(0).

Reduction of $Al_2(MoO_4)_3$. A 20-nm octahedral MoO_3 thin film supported on planar alumina was calcined at 300 °C for 18 h to obtain a film containing $Al_2(MoO_4)_3$ (see Figure 3c,d). The sample was reduced in hydrogen at 350 °C while being monitored by *in situ* Raman spectroscopy (Figure 9). As the hydrogen reduction proceeds, peaks at ~932 and 368 cm^{-1} (marked by arrows in Figure 9) appear and increase in intensity, signifying the growth of $Mo_7O_{24}^{6-}$ (see above). Since the Raman spectra were recorded under identical conditions and the intensities of the peaks due to the $Al_2(MoO_4)_3$ do not appear to change, one may infer that the $Al_2(MoO_4)_3$ is not being converted into the new $Mo_7O_{24}^{6-}$ species. It is unlikely that the sample was completely $Al_2(MoO_4)_3$ but likely contained some amorphous molybdenum oxide, which then converted into the heptamolybdate species during the reduction process, similar to what occurred on the 4 nm thick sample following reduction (see above). The

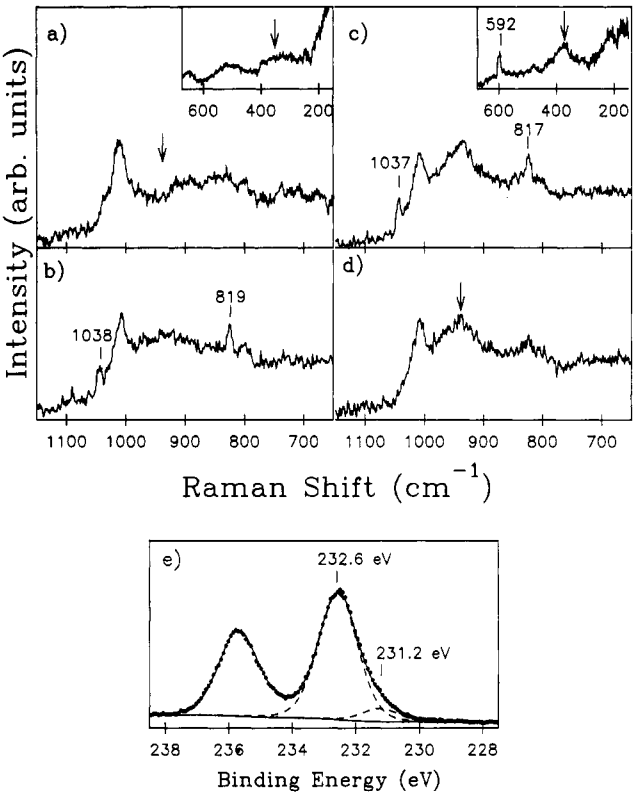

Figure 9. Series of *in situ* LR spectra following the H_2 reduction at 350 °C of a ~20-nm molybdenum oxide/planar alumina thin film containing $Al_2(MoO_4)_3$. Arrows mark the position of growth of new peaks: (a) oxide precursor calcined at 300 °C for 18 h; (b) introducing H_2 at 350 °C; (c) 19 h H_2 reduction; (d) 19 h H_2 reduction at 350 °C, introduce N_2 into reaction cell. The labeled peaks at 1038, 819, and 592 cm^{-1} are due to hydrogen gas in the reaction cell. They are transitory in nature and vanish from the spectra as soon as N_2 has been introduced into the quartz cell. (e) Mo(3d) XP spectrum taken following reduction. Only $Mo(3d_{5/2})$ spin–orbit components are shown for clarity.

photoelectron spectrum following reduction shows that the sample is largely (>90%) Mo(VI) in nature with a small contribution from a Mo(V) peak at 231.2 eV (see Table I). Since both $Al_2(MoO_4)_3$ and the ion $Mo_7O_{24}^{6-}$ have molybdenum in the +6 oxidation state and surrounded by similar numbers of oxygen atoms, one would expect both species to have virtually the same binding energy. Since $Al_2(MoO_4)_3$ has a reported binding energy of 232.6 eV,[17] it would be impossible to distinguish the two species solely on the basis of their Mo(3d) spectra. In any case, the formation of $Al_2(MoO_4)_3$ resulted in much less reduction occurring, perhaps caused by a disruption in the formation of Mo(IV) and Mo(V) oxides.

Discussion

Analysis of Calcined Molybdenum Oxide Thin Films. A number of different molybdenum oxide species and structures are known to reside on the calcined catalysts. The likelihood of a given species existing following calcination is dependent on the impregnation conditions, type of support and its surface area, molybdate loading, and the calcination time and temperature. Monomeric species are believed to predominate at low loadings, yielding polymeric species and $Al_2(MoO_4)_3$ at intermediate loadings and multilayer or bulk MoO_3 at loadings in excess of a monolayer.[17,27,30] The behavior of the catalyst toward further pretreatments such as reduction and sulfidation is influenced by these surface oxides. XPS investigations of the calcined surface species has been largely hampered by the insulating properties of the γ-alumina substrate, unreliable charge referencing, and inadequate charge compensation devices. This necessitates extremely careful work under well-controlled conditions in order to yield useful and reproducible results.

XPS Spectra. The molybdenum photoelectron spectra presented in Figure 1a are quite insensitive to the changes in the corresponding surface molybdates. This is not particularly unusual considering that the valence state of all molybdenum in the surface species is VI and XPS analysis of molybdenum compounds appears insensitive to changes within the oxidation state. However, a change in the photoemission spectrum with molybdenum oxide thickness has been observed as evidenced by the decreasing breadth of the photoelectron peaks on the alumina- and graphite-supported specimens as the oxide thickens (see Figure 1a). A broadened Mo(VI) (fwhm = 1.55 eV) 3d component has also been observed *on a conducting substrate* during thermal reduction of MoO_3 in flowing nitrogen and hydrogen.[22] The data in Figure 2 show that there is a change in the fwhm for Mo(VI) oxide species with molybdenum thickness which cannot be attributed to broadening due to surface charging on nonconducting substrates. The lack of any asymmetry in the XPS spectral envelopes militates against an interpretation of this broadening as due to two or more separate chemical phases. Instead, we suggest that the sputter deposition process used to prepare these films favors the formation of islands and clusters of varying atomic dimensions and that binding energies of these small clusters will vary slightly from that of crystalline MoO_3. Clusters will carry differing numbers of oxygen atoms depending on the aggregate size, the likelihood of anion vacancies at corners or edges, and the degree of bonding to the substrate. These features will influence the local electronic environment that the molybdenum atoms see and ultimately the measured binding energies. This type of low-ordered structure is best represented by the term "amorphous". However, one cannot completely rule out the existence of multiple Mo(VI) species which cannot be resolved by XPS as a possible explanation for the peak broadening effect.

There have been several reports in the literature regarding broadened Mo(3d) peak widths for supported molybdenum oxides compared to the peak widths of bulk (unsupported) MoO_3. Most of these studies have dealt with alumina as the carrier. Some of the papers have ascribed the Mo(3d) peak broadening either to metal–support interactions[48,49] or to possible surface charging effects,[17,48] while others do not offer any explanation.[50] Other groups have been more explicit in their explanation for the peak broadening. Delmon's group ascribed the peak broadening in Co–Mo/γ-alumina catalysts[51] to be due to the presence of multiple molybdenum oxide species which might include a Mo(VI) monolayer species, a Mo(V) species, a polymolybdate form, a bulk MoO_3 phase, or multilayers of MoO_3-like species, depending on the loading. The presence of a Mo(V) species can probably be eliminated since its binding energy has recently been clearly resolved from the binding energy of Mo(VI) oxide species.[22,26,46] Ratnasamy[52] has proposed that two Mo(VI) species may be present: one which is easily reducible and the other which is more difficult to reduce. The two species to which he refers may very well be an octahedral Mo(VI) species and $Al_2(MoO_4)_3$ or a tetrahedral surface species, respectively, since these structures would exhibit the aforementioned types of reduction behavior. Hercule's group has tried to prove that all published reports of Mo(3d) broadening effects observed on γ-alumina substrates can be attributed solely to surface charging.[17,26,30,45] Since photoemission lines from both Mo(3d) and Al(2p) show peak broadening, and no change in work function is expected for the alumina carrier, they allege that surface charging alone must be responsible for the observed peak broadening. While the basis of their argument is sound, it does not explain the results reported on calcined thin film catalysts, particularly on graphite substrates where no charging is present. Nor does it account for the broadened Mo(VI) oxide present on the thermally reduced films supported on conducting substrates of molybdenum metal and graphite, as well as alumina.[22]

The cited references show that there is some precedence in the literature for peak broadening as a function of catalyst loading (film thickness). Admittedly, it is very difficult to distinguish or separate the charge broadening effects from the noncharge broadening effects on alumina-supported catalysts. However, the limited literature references plus our results would imply that there is a noncharging effect which in our case may be a function of molybdate thickness, of substrate type, or a combination of the two factors.

LRS Data. Different properties of the planar alumina-supported molybdenum oxides are revealed in the Raman spectra through their peak shape, the position of the high-frequency band (ν_{sym}(Mo–O)) and additional spectral bands, and the thickness (loading) of the molybdate. These features provide information as to the identity of the molybdate(s) (chain length or cluster size) and their coordination geometry and the degree of surface hydration, and they indicate possible interactions between the molybdate and the carrier. Each of these ideas will be discussed as they apply to supported molybdenum oxides in general and specifically to the thin-film results.

(*a*) *Broadness of the ν_{sym}(Mo–O) Band.* The majority of the spectra in Figure 1b show a broadened band due to the ν_{sym}(Mo–O) stretching frequency at ~950 cm^{-1}, which was ascribed to octahedrally coordinated surface molybdates. Molybdenum oxide compounds exist with either octahedral, MoO_6, or tetrahedral, MoO_4, symmetry. Many researchers use the Raman spectra of pure compounds as a tool to characterize the molybdate species found on supported catalysts.[1,2,17,20,21,29,31,39,53-57] This involves either the use of crystalline compounds such as the catalyst precursor $(NH_4)_6Mo_7O_{24}\cdot 4H_2O$, MoO_3, Na_2MoO_4, or $Al_2(MoO_4)_3$ or the use of aqueous anions $Mo_7O_{24}^{6-}$, $Mo_8O_{26}^{4-}$, or MoO_4^{2-} as appropriate models. Some researchers feel the use of the aqueous anions is more appropriate since the supported catalysts are frequently hydrated due to air exposure.[18,20,28,29,54,57-59] It is important to realize that while tetrahedral and octahedral coordinations are the two geometries of molybdenum oxide compounds, they represent the two idealized structures for supported catalysts. It is quite likely that both structures may be present on the calcined surface. Furthermore, bonding of the molybdate to surface hydroxyl groups on alumina or silica will distort symmetries and cause changes in bond lengths and bond strengths which will result in splitting of Raman spectral peaks and shifts in band frequencies relative to the crystalline compounds or free ions as well as changes in the relative peak intensities compared to the crystalline reference compounds or free anions.

Sharp spectral peaks are associated with crystalline compounds or free (solvated) anions. The broadness of the peaks may indicate a lack of crystallinity or order for the surface molybdates.[2] This would be in line with ideas proposed for the XPS results. The broadness of the ν_{sym}(Mo–O) may be due to the spreading of the molybdenum oxide following calcination to form a one- or two-dimensional monolayer or the influence of surface hydration which leads to solvation of the supported molybdate.[28,53] Since most of the film thicknesses greatly exceed monolayer coverage, the former effect is unlikely to be important here. The latter effect is a more reasonable explanation for the thin-film results, particularly the graphite-supported films, although some contribution from spreading or interaction with alumina hydroxyl groups is also possible on the thinnest films. While the thin-film samples were stored in a desiccator prior to analysis, the surface hydration is possibly caused by brief air exposure of the samples prior to and during Raman analysis.

(*b*) *Position of the ν_{sym}(Mo–O) Band and the Presence of Other Bands.* One of the most obvious features of the spectra presented in Figure 1 is the similarity of the spectra at molybdate thicknesses up to 14 nm. The spectra are relatively simple, displaying a band at 950 cm^{-1} assigned to the ν_{sym}(Mo–O) frequency, a second band at ~880 cm^{-1} assigned as the ν_{asy}(Mo–O–Mo) frequency, a broad feature at ~350 cm^{-1} assigned as δ(Mo–O) (bend) (seen on the 8- and 14-nm specimens), and a broad band at >200 cm^{-1} assigned as δ(Mo–O–Mo) (seen on the 8 nm thick film). The assignment of these fundamentals is in line with literature reports.[28,29,31] The ν_{sym}(Mo–O) band is used as the diagnostic tool for determining the molybdate identity because it is usually the most intense band in the spectrum, and it has been shown to be sensitive to changes in the coordination geometry, the degree of surface hydration, and the molybdenum chain length. This fundamental typically lies in the range ~950–1006 cm^{-1} for octahedrally coordinated molecules and from ~918 to 945 cm^{-1} for tetrahedrally coordinated molecules.[1,2,20,28,31,53] However, there is some discrepancy in the literature over these assignments due to overlap in the frequencies for octahedral and tetrahedral symmetries.[1,2,55] The position of this band shifts to lower frequencies as the degree of hydration increases, with shifts on the order of 15–45 cm^{-1} being reported.[28,29,54] The ν_{sym}(Mo–O) band shifts to higher frequencies as the length of the molybdate chain increases; vis., $MoO_4^{2-} \rightarrow Mo_7O_{24}^{6-} \rightarrow Mo_8O_{26}^{4-} \rightarrow SiMo_{12}O_{40}^{4-}$ yields ν_{sym}(Mo–O) = 897 → 943 → 965 → 980 cm^{-1}.[31,39] For these reasons one should exercise caution in assigning molecular symmetries based solely on the position of the ν_{sym}(Mo–O) band. The spectra shown in Figure 1 are characteristic of octahedrally coordinated polymolybdate structures such as Mo_7O_{24}, but the spectra appear to be somewhat broader (~970–650 cm^{-1}) and less defined than many literature spectra for this species.[28,39,57] This additional broadness may indicate the presence of a tetrahedral molybdate in addition to the octahedral species. A tetrahedral molybdate may be stabilized by bonding to available surface hydroxyl groups on the planar alumina support. Therefore, it is possible that the Raman spectra may yield a composite of surface tetrahedral species and multilayer octahedral species. In the case of the graphite carrier, such an interaction with the molybdate is not possible because there are no available surface hydroxyl groups for bonding. This is supported by the aqueous ammonia results which show the (essentially) complete removal of a ~10 nm thick calcined molybdate film. Thus, if a second molybdate species does not exist on the graphite-supported thin films, it would likely have octahedral geometry.

(*c*) *Thickness of the Supported Molybdate.* The position of the terminal ν_{sym}(Mo–O) is known to change as a function of the molybdate loading on alumina-supported catalysts.[2,17,21,53] This change in ν_{sym}(Mo–O) is explained by a model which describes the change from monomeric species into polymeric surface species as a function of increasing catalyst loading. Under standard conditions, wet impregnation methods are believed to largely yield isolated monomers of the type MoO_4^{2-} at low molybdenum loadings. As the loading increases, either polymeric molybdates may form through the condensation of monomers on adjacent surface sites via bridging water molecules or they may form through a combination of higher surface molybdenum concentrations and a lowering of the PZSC (point of zero surface charge) of the support, both of which favor the formation of polymeric species.[20,28] After monolayer coverage is reached, the molybdate species is (presumably) completely dispersed over the catalyst surface in a monolayer so that the addition of excess molybdate would be converted into bulk MoO_3. One potential flaw in this scheme is that some authors working at loadings below one monolayer may prejudice their interpretations because they *expect* to find tetrahedrally coordinated species on their carrier surfaces at these concentrations. If the molybdate does not adsorb homogeneously on the catalyst surface during impregnation or it does not spread uniformly during calcination, clustering may occur to form two- or three-dimensional polymolybdates or bulk MoO_3 at concentrations well below one monolayer. Despite these problems, this model has adequately explained a large number of reported results.

In the work on thin-film supported molybdate catalysts it is, therefore, unusual to find the ν_{sym}(Mo–O) position invariant of the thickness (loading) of the catalyst on both alumina-and graphite-supported (not shown) thin films. As previously mentioned, the Raman results seem to suggest that a hydrated, octahedral polymolybdate species exists throughout the range of thicknesses studied here, with bulk MoO_3 emerging at the highest thicknesses. The mode of sample preparation (i.e., ion beam deposition) may be responsible as explained below.

In wet impregnation methods, factors such as the solution pH controls the nature of aqueous molybdate species, while the carrier material and its PZSC largely control the type of molybdate (i.e., monomer vs polymer and Mo_7 vs Mo_8) which is initially adsorbed.[1,2,28] Of these factors, only the nature of the support (i.e., planar alumina or graphite) has a large influence on the molybdate structure formed following calcination on the ion beam deposited thin films. Aggregate formation on the thinnest samples (i.e., 2 and 4 nm) may occur because interactions between molybdenum species are more favorable than interactions between the molybdate and the alumina support. This may be due in part to a lack of sufficient surface hydroxyl groups necessary to bond strongly with the molybdates. Inhomogeneity of the planar alumina support, as evident by the appearance of occasional patches of bulk MoO_3 observed at most thicknesses, may also be responsible for facilitating clustering of the molybdenum into polymeric molybdates. At higher thicknesses (i.e., >8 nm) where multilayers of molybdate might form, one would expect to see bulk MoO_3. The absence of the bulk oxide until thicknesses of ~20 nm are reached may be due to the tendency of the amorphous species to take up water, thereby solvating the molybdate film. On the graphite-supported specimens, clustering of the molybdenum would be favored at all thicknesses due to unfavorability of solid–solid wetting processes occurring on supports such as silica and (probably) graphite.[57,60]

The behavior of the planar alumina-supported samples to extended calcination at 300 °C is similar to some work carried out previously by Zingg et al.[17] In this work they observed that a 20 wt % MoO_3/γ-Al_2O_3 catalyst showed partial conversion into $Al_2(MoO_4)_3$ and "interaction species" at a calcination temperature of ~600 °C with more extensive conversion occurring at 700 °C. Formation of $Al_2(MoO_4)_3$ has been reported to occur at temperatures of 500 °C during calcination of near monolayer loadings on γ-alumina substrates,[18,20] but not at temperatures as low as 300 °C as found on the planar alumina-supported catalyst (Figure 3). Aluminum molybdate may be considered to form in the subsurface of the aluminum; for example, within Al^{3+} octahedral vacancies in the spinel structure of γ-alumina[18] or perhaps in micropores where the tetrahedral molybdate is already surrounded at three of the four sites by Al_2O_3.[53] This requires some transport or diffusion of the molybdate species into the alumina lattice. Such processes require high temperatures (≥500 °C) normally observed during aluminum molybdate formation. The planar alumina substrates used in this work may be classified as an amorphous alumina.[61–63] Impregnation of ruthenium chloride in planar films has been shown to preferentially occur at defect sites on the surface associated with scratches.[62] It therefore seems possible that the thermally grown planar films permit more intimate contact between the two oxide phases at surface defects, which facilitates aluminum molybdate formation. This may lessen the temperature necessary for conversion of Al_2O_3 and molybdenum oxide into $Al_2(MoO_4)_3$ on a planar alumina surface than on a γ-alumina surface.

Reduction of Thin-Film Molybdenum Oxides. The 2 nm thick amorphous Mo(VI) oxide specimen shows no evidence of reduction by XPS. This would indicate that this molybdenum species was bonded strongly to the alumina substrate and resisted reduction at 350 °C. The 4 nm thick planar alumina-supported molybdenum oxide film represents the lower limit in oxide thickness over which H_2 treatment results in an obvious conversion of the calcined precursor into a new product(s) observed by LRS. Besides the two oligomers, $Mo_7O_{24}^{6-}$ and $Mo_6O_{19}^{2-}$ (tentative), there is evidence of some reduced species (MoO_2). The formation of these octahedral crystalline species from an amorphous molybdate (the 4 nm thick film) indicates that the H_2 treatment involves some aggregate formation and/or restructuring of the amorphous material. While evidence for aggregate formation during reduction has been proposed, it is normally associated with the breaking of Mo–O–Al bonds to free the molybdate from the substrate so that clustering can occur.[19,29,64,65] In addition, aggregate formation is usually associated with a decrease in the valence state of molybdenum. The Raman data do indicate the formation of some reduced molybdenum species (MoO_2), and the XPS data show a mixture of oxides present with a Mo(VI) species dominating at 232.6 eV but with additional lower oxidation state species also present. However, the majority of the Raman spectra indicate the presence of two crystalline materials, ($Mo_7O_{24}^{6-}$ and $Mo_6O_{19}^{2-}$), which have an oxidation state of VI and are octahedrally coordinated. The stability of these two polyanions to the reducing environment is perplexing. Octahedrally coordinated species which do not bond strongly to the alumina support are expected to reduce readily in H_2. It is possible that at 350 °C reduction is slow and difficult to observe in the Raman spectra. Perhaps excess surface hydroxyl groups or adsorbed water has combined with the molybdate species to inhibit the reduction. It has been reported that at reduction temperatures below 450 °C some adsorbed water is strongly retained by the alumina support and this water may facilitate oxidation of the surface species or retard their reduction.[66,67]

Reduction of Octahedral MoO_3. The results from this study on the extended reduction (≥12 h) of octahedral MoO_3 showed little difference with those reductions carried out for shorter periods of time at temperatures >600 °C. Thus, it appears that MoO_3 is unlikely to reduce completely to molybdenum(IV) oxide. Reduction of octahedral molybdenum oxide at 500 °C for periods exceeding 12 h in environments of flowing nitrogen and hydrogen and *in vacuo* reduction yields only ~30% molybdenum(IV) oxide as crystalline MoO_2 (BE = 229.2 eV) and ~20% as nondiscrete molybdenum(IV) oxide (BE = 230.1 eV), regardless of the reduction environment. The other ~50% is made up of molybdenum(V) oxide and a molybdenum(VI) oxide (BE = 232.6 eV) (see Table I). One possible explanation for the discrepancy in results between the present study and the work in refs 17 and 30 may lie in the difference in spectral resolution achieved between the two groups. The Mo($3d_{5/2}$) fwhm values used in the present work for standard samples and test results are much narrower than those reported by other groups examining the reduction of molybdenum oxides.[17,26,30,45,68–70] Angular-dependent XPS results (not shown) performed on all of the specimens show that the composition is uniform throughout the mean analysis sampling depth (~2–6 nm). This means that gradient effects, inhomogeneity, or particle size effects are not likely the cause of the discrepancy.

In ref 22, two possible mechanisms were suggested to explain the presence of the Mo(IV) and Mo(V) states—the formation of *discrete* tetrahedral species or the production of *nondiscrete* tetra- and pentavalent states formed through crystallographic shear processes. The lack of *in situ* Raman evidence for tetrahedral species on any of the thicker (≥15 nm) specimens lends favor to nondiscrete phases rather than discrete structures. However, the lack of spectral evidence for potential tetrahedral components may be due to the greater sensitivity of Raman scatter for MoO_3, which has been estimated as 15 (71) or 50–100[39,72] times greater than for surface molybdates. This means that discrete tetrahedral structures may still be present but unobserved by Raman analysis.

These longer duration (≥12-h) reduction studies produced relative concentrations of four oxide species, MoO_2, Mo(IV),

Mo(V), and Mo(VI), which were similar to those produced after thermal decomposition of octahedral MoO_3 at 600–730 °C for 1 h.[22] A similar result was also observed for octahedral MoO_3 films supported on graphite reduced at 350 °C in hydrogen for >9 h. Other groups have observed a similar constant peak shape in the Mo(3d) envelope as we have reported, although individual peak-fitting parameters have varied from group to group. Cimino et al.[50] have observed a Mo(3d) envelope similar to Figure 6a for MoO_2 "taken from the bottle" as well as for MoO_3 reduced in 500 Torr H_2 at 400 °C. Hercules' group[17,30,68] has also obtained similar spectral line shapes for γ-alumina-supported MoO_3 following H_2 reduction at 550 and 350 °C and on Co–Mo–alumina catalysts reduced under similar conditions. Kim et al. reported several similar results for "MoO_2" and for ion-dosed MoO_3.[73] Grünert et al.[70] studied the thermal decomposition of MoO_3 under Ar and reported spectral results very similar to those reported here as well as tabulated concentrations in agreement with our past and present results. The reproducibility of these observations taken from a variety of sources and the lack of any experimental evidence (other than by XPS) to identify the structures of both the Mo(IV) and Mo(V) oxides leads us to believe that these intermediate oxidation states observed by XPS are *nondiscrete in nature*. The similarity of products obtained by these groups using a variety of conditions can be explained through crystallographic shear processes as will be explained below.

The O/Mo concentration ratio on the reduced surface is 2.2 ± 0.2. From the relative concentration of molybdenum oxidation states found in Table II, and O/Mo ratio of 2.3 is calculated, assuming 3, 2.5, and 2 as O/Mo stoichiometries for Mo(VI), Mo(V), and Mo(IV) states. This tends to support the analysis proposed above for multiple molybdenum states.

The narrowness of the MoO_2 spin–orbit peaks ($Mo(3d_{5/2})$ = 0.64 and 0.74 eV) demands attention. Narrow spectral peak widths are usually only observed on metallic surfaces. The structure of molybdenum dioxide consists of alternately longer (3.11 Å) and shorter (2.51 Å) Mo–Mo bond distances than in molybdenum metal itself (2.94 Å).[43] Metal–Metal bonding occurs through σ–σ overlap between the Mo(4d) orbitals of the two closely spaced molybdenum atoms.[74,75] The orbital overlap is strong enough to split the σ(Mo–Mo) band into bonding and antibonding bands. The MoO_2 d^2 configuration yields a partially filled Mo–O(π^*) conduction band which merges with the Mo–Mo(σ^*) band and results in the metallic conductivity. The narrowness of the Mo(3d) spin–orbit species may then be envisioned as being due to the metallic character of the MoO_2 compound. Following ejection of a core-level electron during the photoemission process, readily available electrons from the metallic conduction band can quickly fill the core hole, resulting in a short core hole lifetime and a narrow spectral line width.

The use of three different gaseous environments for the decomposition and reduction of octahedral MoO_3 requires comment. Many catalytic processes including HDS use H_2 as the sole reducing/activating agent for the molybdate catalysts.[6] In the specific case of HDS H_2 is usually added into the sulfiding stream. The accepted mechanism of reduction for MoO_3 and supported molybdates involves the adsorption and dissociation of hydrogen molecules onto the oxygen atoms, followed by the release of a water molecule and the concomitant lowering of the molybdenum valence state.[29,76–78] Thermal decomposition of MoO_3 and supported molybdates in inert gases such as nitrogen[22] and argon[70,79] or *in vacuo*[80,81] leading to reduced (<Mo(VI)) molybdenum species is well documented. Similar Mo(3d) chemical shifts to those found after reduction with hydrogen have been observed for the inert gas and *in vacuo* treatments.[70,79,81] The mechanism of reduction in inert gases and *in vacuo* treatments[70,79,81] The mechanism of reduction in inert gases and *in vacuo* heating likely involves the diffusion of lattice oxygen from the bulk material through defects and vacancies to the surface

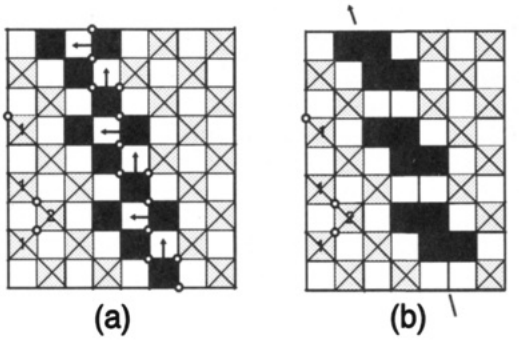

Figure 10. Schematic diagram of an idealized MoO_3 lattice of corner-shared octahedra which undergoes reconstruction through the formation of a crystallographic shear plane.[90] (a) Arrows indicate the direction of the shear process. Open circles indicate oxygen vacancies. Octahedra involved in the reconstruction are darkened. Isolated vacancies representing Mo(IV) and Mo(V) phases are denoted by the numerals 1 and 2, respectively. (b) Reconstructed phase showing the removal of anion vacancies along the shear plane. Multiplicity of states is apparent with MoO_2, Mo(IV), Mo(V), and Mo(VI) simultaneously present.

where it combines with adsorbed surface hydrogen to form hydroxyl groups and water, or it may combine to form molecular oxygen and then be carried off in the inert gas stream or into the instrument vacuum. The driving force behind this process is the stabilization of the lattice by the removal of point defects through the formation of crystallographic shear planes. While this process is probably slower and gentler than H_2 reduction, at the temperatures and times chosen (500 °C for >12 h or >600 °C for 1 h), the results would indicate that similar reduction products are obtained regardless of the gaseous environment (Table II).

To understand the reason for the broad spectral Mo(3d) envelope containing multiple states, one must examine the structures of the starting material (MoO_3) and the end product (MoO_2) and the mechanism through which the transformation takes place. MoO_3 consists of a bilayer of distorted corner-linked MoO_6 octahedra running parallel to the [010] direction; each bilayer is held together by weak van der Waals forces providing easy cleavage along (010) planes.[43,82,83] MoO_2 is composed of strings of MoO_6 octahedra joined by edges along [100] and connected by corner-sharing into a three-dimensional structure.[84] The mechanism which governs the decomposition of MoO_3 and the rearrangement from primarily corner-sharing to edge-sharing octahedra involves crystallographic shear processes. These ideas, as proposed by Haber,[85] suggest that a large number of point defects in the MoO_3 lattice can be eliminated through the formation of a crystallographic shear plane. The point defects may be generated at random through reduction processes. These defects can be generated through heating in a variety of gaseous environments including *in vacuo*, H_2, and inert gases. After a sufficiently high concentration of defects is present, the lattice collapses through crystallographic shear and rearranges to form a more stable structure. The edge-linked structure formed through crystallographic shear has a lower energy than the corner-linked structure containing the oxygen vacancy.[86] There may exist a finite number of isolated vacancies in the presence of crystallographic planes.[82] These random vacancy sites should carry reduced molybdenum valences such as Mo(V) for singly vacant sites or Mo(IV) for doubly vacant sites. At the same time, removal of aggregates of point defects through crystallographic shear would continue to form MoO_2. A certain degree of reduction would correspond to a given density of shear planes[66] and a finite number of anion vacancies representing a nonstoichiometric phase. Figure 10 shows a schematic diagram of an idealized MoO_3 lattice of corner-shared octahedra which reconstructs through the formation of a crystallographic shear plane to eliminate a series of point defects. At the boundary of the crystallographic shear plane now lies edge-joined octahedra in a MoO_2-like microstructure. Hence, MoO_2, Mo(IV), Mo(V), and Mo(VI) states may be

simultaneously present within the same structure as observed in the XPS spectra.

A series of molybdenum oxide phases with complex, but well-defined, stoichiometries of Mo_nO_{3n-1} exist within the range of $Mo_{2.929}$ to $Mo_{2.875}$ with $n = 8$–12, 14.[87] These phases have stringent tolerances for oxygen vacancies and will reconstruct into new phases via shear processes if the number of vacancies exceeds a certain concentration. These phases are defined shear structures, which may contain distinct crystallographic structures and Raman spectra.[88] The lack of Raman spectra corresponding to any of these known phases necessarily negates their existence in this work.

Aqueous ammonia has been shown to dissolve octahedral molybdenum trioxide. Aqueous ammonia treatment of a sample of MoO_3/Mo reduced in hydrogen at 500 °C for 14 h (Figure 7) revealed that some MoO_3 was still present on the sample following reduction. Moreover, a substantial amount of other nonoctahedral Mo(VI) species is shown to still reside on the reduced specimen. This species produces a broadened Mo(VI) spectral peak (fwhm = 1.55) which results from reduction of octahedral MoO_3. The breadth of this Mo(VI) spectral peak suggests that it *may* be of similar nature to Mo(VI) species observed as thin films supported on planar alumina and graphite substrates.

The pressed disk of MoO_3 behaved quite differently than the supported octahedral MoO_3/Mo films toward thermal reduction in H_2 at 500 °C. XPS results show that molybdenum in the disk is effectively reduced to the zero valence state, while the films do not show evidence of reduction lower than the Mo(IV) state at 230.1 eV. XPS and LRS analysis of the precursor materials indicated that both materials were identical to crystalline (bulk) MoO_3 and thus were expected to behave similarly to the reduction treatments. A direct support interaction of the type normally associated with Mo/Al_2O_3 catalysts is not present due to the thickness of the films.

One must look for other reasons to explain the observed results. One possible explanation may be due to the differences in morphology between the pressed pellet and the thick film. In the mechanically pressed pellet, a random orientation of all possible crystal faces of MoO_3 would likely be achieved with crystallites of varying size forced together. Given the layered structure of MoO_3 (bilayer of distorted corner-linked MoO_6 octahedra running parallel to the (010) planes and held together by weak van der Waals forces providing easy cleavage along these planes),[43,83] this random array would yield many imperfections including misalignment between layers and point defects. Such a structure should present a facile pathway for H_2 reduction through vacancy and anion diffusion. Indeed, reduction of bulk MoO_3 to the metallic state has been observed under similar reaction conditions and temperatures.[89]

With regard to the thin films, nucleation and growth of the oxide film on the metal substrate may impart more ordered growth of the MoO_3 layers with a greater structural density and fewer defects. An ordered structure should be more impervious to diffusion processes (compared to the pressed pellet) during reduction, retarding reduction at the +4 state under the same reaction conditions which reduced the pelletized sample to the metallic state.

Reduction of $Al_2(MoO_4)_3$. Raman analysis of the 20 nm thick film originally containing $Al_2(MoO_4)_3$ shows evidence of the formation of $Mo_7O_{24}^{6-}$. These results are contrary to literature studies which showed that reduction of a tetrahedral molybdenum species, $Al_2(MoO_4)_3$, results in the formation of a Mo(V) species.[17] Our results show that the tetrahedral $Al_2(MoO_4)_3$ species is quite resistant to reduction. In fact, the small contribution of a reduced molybdenum species observed in the XP spectra of the 20-nm film is believed to result from reduction of the non-$Al_2(MoO_4)_3$ species present on the sample (i.e., the amorphous envelope underneath).

The lack of any appreciable reduction of the aluminum molybdate phase is probably due to the reduction temperature chosen, 350 °C. It has been reported by Massoth[76] that reduction of aluminum molybdate in H_2 requires a temperature of at least 500 °C. More puzzling is the formation of the heptamolybdate species under a reducing atmosphere. Since the experiment was conducted *in situ* under flowing high-purity, dried H_2, it is highly unlikely that moisture or oxidation may have played a role in the reaction. It is difficult to understand why a Mo(VI) species would evolve under H_2 exposure. Even under mild H_2 reduction conditions some decrease in the molybdenum oxidation state should be expected. As mentioned above, polyanion formation is possible, but not usually without reduction in the molybdenum valence state. According to the XPS spectra, very little reduction has occurred. The presence of strongly adsorbed water on the surface of the planar alumina may again be inhibiting or reversing the reduction process.

Conclusions

1. A range of Mo($3d_{5/2}$) peak widths have been found for molybdenum(VI) oxide supported on planar alumina and graphite. These peak widths may be influenced by molybdenum oxide aggregate sizes and the local electronic environment surrounding each molybdenum atom which are in turn determined by the film thickness. Alternatively, the increasing peak widths may indicate multiple unresolved Mo(VI) species.

2. Formation of aluminum molybdate on thin film catalysts has been observed at much lower temperatures than are normally found using conventional preparation techniques. A possible explanation for this occurrence may be due to the large number of defects associated with the amorphous planar alumina substrate, which would facilitate contact between the molybdate and alumina phases and lower the required reaction temperature.

3. The reduction products from thin-film, planar alumina-supported molybdenum(VI) oxides are dependent on the thickness of the oxide layer and the presence of $Al_2(MoO_4)_3$, which is resistant to reduction at 350 °C.

4. Reduction of supported octahedral MoO_3 in H_2 or N_2 or *in vacuo* at 500 °C for extended periods yields a mixture of MoO_2 and higher Mo(3d) oxidation states. In constrast, unsupported octahedral MoO_3 reduces largely to molybdenum metal, with varying amounts of higher oxides.

References and Notes

(1) Ng, K. Y. S.; Gulari, E. *J. Catal.* **1985**, *92*, 340.
(2) Cheng, C. P.; Schrader, G. L. *J. Catal.* **1979**, *60*, 276.
(3) de Beer, V. H. J.; van der Aalst, M. J. M.; Machiels, C. J.; Schuit, G. C. A. *J. Catal.* **1976**, *43*, 78.
(4) Ahuja, S. P.; Derrien, M. L.; LePage, J. F. *Ind. Eng. Chem. Prod. Res. Dev.* **1970**, *9*, 272.
(5) Brown, F. R.; Makovsky, L. E.; Rhee, K. H. *J. Catal.* **1977**, *50*, 385.
(6) Gates, B. C.; Katzer, J. R.; Schuit, G. C. A. In *Chemistry of Catalytic Processes*; Ciofalo, R., Marshall, J., Leap, B., Eds.; McGraw-Hill: New York, 1979; Chapter 5, p 390.
(7) Groot, C. K.; de Beer, V. H. J.; Prins, R.; Stolarski, M.; Niedzwiedz, W. S. *Ind. Eng. Chem. Prod. Res. Dev.* **1986**, *25*, 522.
(8) Duchet, J. C.; van Oers, E. M.; de Beer, V. H. J.; Prins, R. *J. Catal.* **1983**, *80*, 386.
(9) Bouwens, S. M. A. M.; Prins, R.; de Beer, V. H. J.; Koningsberger, D. C. *J. Phys. Chem.* **1990**, *94*, 3711.
(10) Topsøe, H.; Clausen, B. S.; Topsøe, N.-Y.; Pedersen, E. *Ind. Eng. Chem. Fundam.* **1986**, *25*, 25.
(11) Daly, F. P.; Brinen, J. S.; Schmitt, J. L. *Appl. Catal.* **1984**, *11*, 161.
(12) Massoth, F. E. *Adv. Catal.* **1978**, *27*, 265.
(13) Hercules, D. M.; Klein, J. C. In *Electron Spectroscopy for Chemical Analysis Applied to Heterogeneous Catalysis, Chemical Analyses*; Windawi, H., Ho, F. F.-L., Eds.; John Wiley and Sons: New York, 1982; Vol. 63, p 147.
(14) Sonnemans, J.; Mars, P. *J. Catal.* **1973**, *31*, 209.
(15) Dufaux, M.; Chem, M.; Naccache, C. *J. Chim. Phys.* **1970**, *67*, 527.

(16) Schuit, G. C. A.; Gates, *Am. Inst. Chem. Eng. J.* **1973**, *19*, 417.
(17) Zingg, D. S.; Makovsky, L. E.; Tischer, R. E.; Brown, F. R.; Hercules, D. M. *J. Phys. Chem.* **1980**, *84*, 2898.
(18) Giordano, N.; Bart, J. C. J.; Vaghi, A.; Castellan, A.; Martinotti, G. *J. Catal.* **1975**, *36*, 81.
(19) Okamoto, Y.; Imanaka, T. *J. Phys. Chem.* **1988**, *92*, 7102.
(20) Stencel, J. M.; Makovsky, L. E.; Sarkus, T. A.; de Vries, J.; Thomas, R.; Moulijn, J. A. *J. Catal.* **1984**, *90*, 314.
(21) Brown, F. R.; Makovsky, L. E.; Rhee, K. H. *J. Catal.* **1977**, *50*, 162.
(22) Spevack, P. A.; McIntyre, N. S. *J. Phys. Chem.* **1992**, *96*, 9029.
(23) Spevack, P. A.; McIntyre, S. *Appl. Catal.* **1990**, *64*, 191.
(24) McIntyre, N. S.; Chan, T. C.; Spevack, P. A.; Brown, J. R. In Hydrotreating Catalysts: Preparation, Characterisation and Performance. *Studies in Surface Science and Catalysis*; Occelli, M., Anthony, R., Eds.; Elsevier: Amsterdam, 1989; Vol. 50, p 187.
(25) McIntyre, N. S.; Chan, T. C.; Spevack, P. A.; Brown, J. R. *Appl. Catal.* **1990**, *63*, 391.
(26) Quincy, R. B.; Houalla, M.; Proctor, A.; Hercules, D. H. *J. Phys. Chem.* **1990**, *94*, 1520.
(27) Giordano, N.; Castellan, A.; Bart, J. C. J.; Vaghi, A.; Campadelli, F. *J. Catal.* **1975**, *37*, 204.
(28) Williams, C. C.; Ekerdt, J. G.; Jehng, J.-M.; Hardcastle, F. D.; Wachs, I. E. *J. Phys. Chem.* **1991**, *95*, 8791.
(29) Seyedmonir, S. R.; Howe, R. F. *J. Catal.* **1988**, *110*, 216.
(30) Li, C. P.; Hercules, D. M. *J. Phys. Chem.* **1984**, *88*, 456.
(31) Payen, E.; Grimblot, J.; Kasztelan, S. *J. Phys. Chem.* **1987**, *91*, 6642.
(32) Vedrine, J. C.; Praliaud, H.; Meriaudeau, P.; Che, M. *Surf. Sci.* **1979**, *80*, 101.
(33) Briggs, D.; Rivière, J. C. In *Practical Surface Analysis*, 2nd ed.; Briggs, D., Seah, M. P., Eds.; John Wiley and Sons: Chichester, 1990; Vol. 1, p 85.
(34) Tanuma, S.; Powell, C. J.; Penn, D. R. *Surf. Interface Anal.* **1991**, *17*, 911.
(35) McIntyre, N. S.; Spevack, P. A.; Beamson, G.; Briggs, D. *Surf. Sci. Lett.* **1990**, *237*, L390.
(36) Shirley, D. A. *Phys. Rev. B* **1972**, *5*, 4709.
(37) Scofield, J. H. *J. Electron Spectrosc. Relat. Phenom.* **1976**, *8*, 129.
(38) Glovebag is a trademark of the "Instruments for Research and Industry, Inc." (I^2R); P.O. Box 159, Cheltenham, PA 19012.
(39) Williams, C. C.; Ekerdt, J. G.; Jehng, J.-M.; Hardcastle, F. D.; Turek, A. M.; Wachs, I. E. *J. Phys. Chem.* **1991**, *95*, 8781.
(40) Bartlett, J. R.; Cooney, R. P. In *Spectroscopy of Inorganic-based Materials*; Clark, R. J. H., Hester, R. E., Eds.; John Wiley and Sons: New York, 1987; p 187.
(41) Schrader, G. L.; Cheng, C. P. *J. Catal.* **1983**, *80*, 369.
(42) Chang, C. H.; Chan, S. S. *J. Catal.* **1981**, *72*, 139.
(43) *Advanced Inorganic Chemistry*, 4th ed.; Cotton, F. A., Wilkinson, G., Eds.; John Wiley and Sons: New York, 1980; p 854.
(44) Grasselli, J. G.; Snavely, M. K.; Bulkin, B. *J. Phys. Rep.* **1980**, *65*, 231.
(45) Yamada, M.; Yasumaru, J.; Houalla, M.; Hercules, D. M. *J. Phys. Chem.* **1991**, *95*, 7037.
(46) *NIST X-ray Photoelectron Spectroscopy Database*, Version 1.0; Wagner, C. D., Bickham, D. M.; Eds.; National Institute of Standards and Technology: Gaithersburg, MD, 1989.
(47) Wagner, C. D.; Riggs, W. M.; Davis, L. E.; Moulder, J. F. In *Handbook of X-ray Photoelectron Spectroscopy*; Muilenberg, G. E., Ed.; Perkin-Elmer, Physical Electronics Division: Eden Prairie, MN, 1979; p 104.
(48) Best, S. A.; Squires, R. G.; Walton, R. A. *J. Catal.* **1979**, *60*, 171.
(49) Edmonds, T.; Mitchell, P. C. H. *J. Catal.* **1980**, *64*, 491.
(50) Cimino, A.; de Angelis, B. A. *J. Catal.* **1975**, *36*, 11.
(51) Gajardo, P.; Grange, P.; Delmon, B. *J. Catal.* **1980**, *63*, 201.
(52) Ratnasamy, P. *J. Catal.* **1975**, *40*, 137.
(53) Medema, J.; van Stam, C.; de Beer, V. H. J.; Konings, A. J. A.; Koningsberger, D. C. *J. Catal.* **1978**, *53*, 386.
(54) Kasztelan, S.; Grimblot, J.; Bonnelle, J. P.; Payen, E.; Toulhoat, H.; Jacquin, Y. *Appl. Catal.* **1983**, *7*, 91.
(55) Wang, L.; Hall, W. K. *J. Catal.* **1980**, *66*, 251.
(56) Kakuta, N.; Tohji, K.; Udagawa, Y. *J. Phys. Chem.* **1988**, *92*, 2583.
(57) Leyrer, J.; Margraf, R.; Taglauer, E.; Knözinger, H. *Surf. Sci.* **1988**, *201*, 603.
(58) Miyata, H.; Tokuda, S.; Ono, T.; Ohno, T.; Hatayama, F. *J. Chem. Soc., Faraday Trans.* **1990**, *86*, 2291.
(59) Okamoto, Y.; Imanaka, T.; Teranishi, S. *J. Catal.* **1980**, *65*, 448.
(60) Leyrer, J.; Mey, D.; Knözinger, H. *J. Catal.* **1990**, *124*, 349.
(61) Cocke, D. L.; Johnson, E. D.; Merrill, R. P. *Catal. Rev.—Sci. Eng.* **1984**, *26* (2), 163.
(62) Halverson, D. E.; Cocke, D. L. *J. Vac. Sci. Technol.* **1989**, *A7* (1), 40.
(63) Fritsch, A.; Légaré, P. *Surf. Sci.* **1987**, *186*, 247.
(64) Nag, N. K. *J. Catal.* **1985**, *92*, 432.
(65) Valyon, J.; Hall, W. K. *J. Catal.* **1983**, *84*, 216.
(66) Ratnasamy, P.; Ramaswamy, A. V.; Banerjee, K.; Sharma, D. K.; Ray, N. *J. Catal.* **1975**, *38*, 19.
(67) Lipsch, J. M. J. G. Thesis, Eindhoven, 1968.
(68) Patterson, T. A.; Carver, J. C.; Leyden, D. L.; Hercules, D. M. *J. Phys. Chem.* **1976**, *80*, 1700.
(69) Clayton, C. R.; Lu, Y. C. *Surf. Interface Anal.* **1989**, *14*, 66.
(70) Grünert, W.; Stakheev, A. Y.; Feldhaus, R.; Anders, K.; Shpiro, E. S.; Minachev, K. M. *J. Phys. Chem.* **1991**, *95*, 1323.
(71) Baltrus, J. P.; Makovsky, L. E.; Stencel, J. M.; Hercules, D. M. *Anal. Chem.* **1985**, *57*, 2500.
(72) Thomas, R.; Mittelmeijer-Hazeleger, M. C.; Kerkhof, F. J. M.; Moulijn, J. A.; Medema, J.; de Beer, V. H. J. In *Proceedings of the Climax 3rd International Conference on Chemistry and Uses of Molybdenum*; Climax Molybdenum: Ann Arbor, MI, 1979; p 85.
(73) Kim, K. S.; Baitinger, W. E.; Amy, J. W.; Winograd, N. *J. Electron Spectrosc. Relat. Phenom.* **1974**, *5*, 351.
(74) Beatham, N.; Orchard, A. F. *J. Electron. Spectrosc. Relat. Phenom.* **1979**, *16*, 77.
(75) Sasaki, T. A.; Soga, T.; Adachi, H. *Phys. B* **1982**, *113*, 647.
(76) Massoth, F. E. *J. Catal.* **1973**, *30*, 204.
(77) Millman, W. S.; Crespin, M.; Cirillo, A. C., Jr.; Abdo, S.; Hall, W. K. *J. Catal.* **1979**, *60*, 404.
(78) Weigold, H. *J. Catal.* **1983**, *83*, 85.
(79) Grünert, W.; Yu, Stakheev, A. Y.; Mörke, W.; Feldhauw, R.; Anders, K.; Shpiro, E. S.; Minachev, K. M. *J. Catal.* **1992**, 269.
(80) Demanet, C. M.; Steinberg, M. *Appl. Surf. Sci.* **1982–83**, *14*, 271.
(81) Topsøe, N.-Y.; Topsøe, H. *J. Catal.* **1982**, *75*, 354.
(82) Gai, P. L.; Boyes, E. D. In *Catalysis Reviews: Science and Engineering*; Bell, A. T., Klier, K., Eds.; Marcel Dekker: New York, 1992; Vol. 34, Nos. 1 and 2, p 13.
(83) Firment, L. E.; Firretti, A. *Surf. Sci.* **1983**, *129*, 155.
(84) Dufour, L. C.; Bertrand, O.; Floquet, N. *Surf. Sci.* **1984**, *147*, 396.
(85) Haber, J.; Marczewski, W.; Stoch, J.; Ungier, L. *Ber. Bunsen-Ges. Phys. Chem.* **1975**, *79*, 970.
(86) Broclawik, E.; Haber, J. *J. Catal.* **1981**, *72*, 379.
(87) *Ionic Crystals, Lattice Defects, and Nonstoichiometry*; Greenwood, N. N., Ed.; Butterworth: London, 1968; p 142.
(88) McCormick, R. L. M.Sc. Thesis, Iowa State University, 1984.
(89) Holl, Y.; Touroude, R.; Maire, G.; Muller, A.; Engelhard, P. A.; Grosmangin, J. *J. Catal.* **1987**, *104*, 202.
(90) Wadsley, A. D. In *Nonstoichiometric Compounds*; Mandelcorn, L., Ed.; Academic Press: New York, 1964.